Y.-W. Lin, S.-S. Li, Z. Ren, and C. T.-C. Nguyen, "Third-order intermodulation distortion in capacitively-driven VHF micromechanical resonators," *Proceedings*, IEEE Int. Ultrasonics Symposium, Sept. 18-21, 2005, pp. 1592-1595.

Third-Order Intermodulation Distortion in Capacitively-Driven VHF Micromechanical Resonators

Yu-Wei Lin, Sheng-Shian Li, Zeying Ren, and Clark T.-C. Nguyen

Center for Wireless Integrated Micro Systems
Department of Electrical Engineering and Computer Science
University of Michigan, Ann Arbor, Michigan 48109-2122, USA

***Abstract*—Substantial increases by more than 22 dB in the third-order input intercept points (IIP_3) of capacitively transduced MEMS-based vibrating micromechanical resonators have been attained by using contour-mode disk geometries to replace previous clamped-clamped beam versions. Specifically, a 156-MHz contour-mode disk resonator with Q = 20,500 exhibits a measured IIP_3 = 19.49 dBm, which is substantially better than the -3 dBm previously measured for a 10-MHz clamped-clamped beam resonator, and which now erases any lingering skepticism regarding the linearity of micro-scale mechanical resonators. Indeed, with IIP_3's about 20 dBm, high Q communication filters using the micromechanical resonators of this work should now be able to replace present-day receive path filters with little degradation (only 0.11 dB) in cumulative receiver IIP_3.**

***Keywords*—microelectromechanical devices, microresonators, interference, intermodulation distortion, filters.**

I. Introduction

Recently, capacitively-driven vibrating micromechanical resonators have been demonstrated with resonant frequencies in the GHz range with Q's still larger than 11,000 [1], making them very attractive as on-chip frequency selecting elements for oscillators and filters in wireless communications. To date, micromechanical filters comprised of several micromechanical resonators coupled mechanically via soft mechanical springs [2] have been demonstrated with highly selective, low insertion loss performance, perhaps suitable for band- or channel-selecting filter banks [3] when translated to higher frequencies. Despite these advantages, efforts to apply micromechanical resonator technology to RF communication circuits have so far been delayed by lingering questions concerning the linearity of these devices, which must be sufficient to maintain the needed minimum cumulative receiver linearity specification for the targeted application (e.g., cellular phone).

The past few years have seen only limited efforts to measure the linearity of micromechanical beam resonators around 10 MHz [4][5], with less than impressive IIP_3's. Pursuant to determining the linearity of higher frequency resonators, this paper presents a complete analytical formulation for the IIP_3 of capacitively-transduced micromechanical disk resonators, and then verifies the formulation via a modified setup that removes measurement instrument nonlinearity (c.f., Fig. 1). Using this setup, an IIP_3 = 19.49 dBm is observed for a 156-MHz contour-mode disk resonator with Q = 20,500, which is substantially better than the -3 dBm previously measured for a 10-MHz clamped-clamped beam resonator [4], and good enough to replace a present-day receive path filter with little degradation (only 0.11 dB) in cumulative receiver IIP_3.

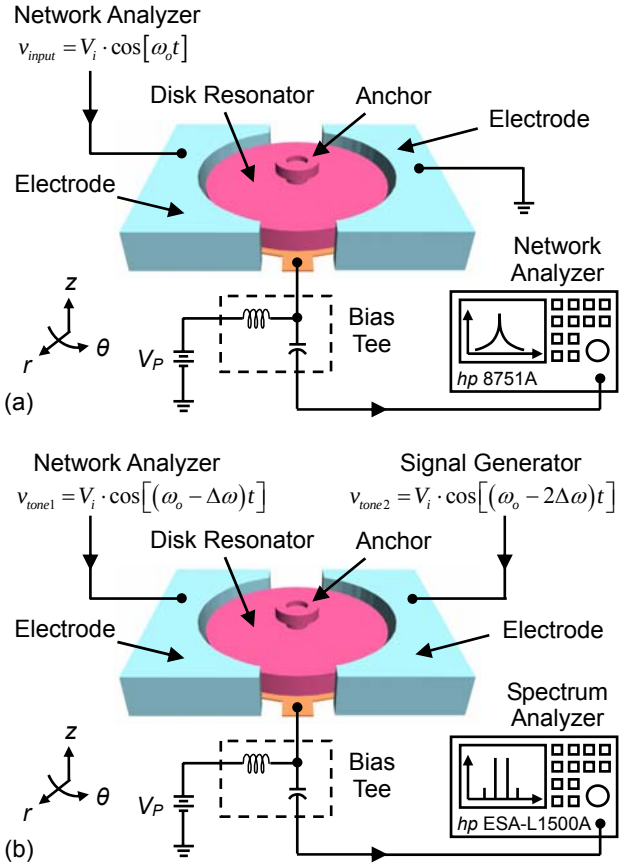

Fig. 1: Perspective-view schematic of a micromechanical disk resonator in (a) a fundamental and (b) an IIP_3 measurement setup.

II. Intermodulation Distortion Fundamentals

Third-order intermodulation distortion (IM_3) for a frequency filter occurs when system nonlinearities allow two strong out-of-band interferers spaced from an in-band frequency ω_o by $\Delta\omega$ and $2\Delta\omega$ (as shown in Fig. 2), to generate an in-band component back at ω_o, corrupting the desired component at ω_o [6]. More quantitatively, an input signal containing the desired fundamental signal plus the two out-of-band interfering signals can be expressed as

$$S_{in} = A\cos\omega_o t + A_1\cos\omega_1 t + A_2\cos\omega_2 t \qquad (1)$$

where A, A_1, and A_2, are amplitudes of the fundamental signal and two interfering signals, respectively. If this signal is sent through a general nonlinear transfer function, given by

$$S_{out} = \alpha_0 + \alpha_1 S_{in} + \alpha_2 S_{in}^2 + \alpha_3 S_{in}^3 + \cdots \qquad (2)$$

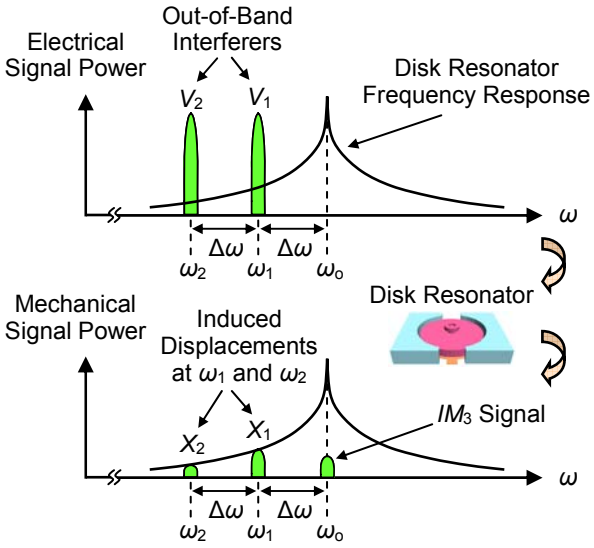

Fig. 2: Schematic description of the mechanism for IM_3 distortion in a capacitively-driven micromechanical resonator.

where α_0, ..., α_n are constants, the resulting output (inserting (1) into (2)), then becomes

$$S_{out} = \cdots + \alpha_1 A \cos\omega_o t + \frac{3\alpha_3 A_1^2 A_2}{4}\cos(2\omega_1 - \omega_2)t + \cdots \qquad (3)$$

where the first term is the fundamental component and the second term is third-order intermodulation component (IM_3), generated via third-order nonlinearity represented by α_3.

Since communication receivers generally operate under interferer environments similar to that depicted in Fig. 2, IM_3 products in the filter passband at $2\omega_1$-ω_2 can be quite troublesome, as they can mask the intended received signal. As such, IM_3 distortion must be constrained below a minimum acceptable value. A useful metric gauging the ability of a system to suppress IM_3 distortion is the third-order input intercept point (IIP_3), defined as the input amplitude at which the extrapolated IM_3 and fundamental output components are equal in magnitude. In general, a larger IIP_3 indicates better linearity and a better ability to suppress interferer-induced IM_3 products, so is preferred for communication systems.

III. Intermodulation Distortion Formulation

Fig. 1(a) presents the perspective-view schematic for a capacitively-driven micromechanical contour-mode disk resonator, embedded in a setup suitable for measuring its fundamental mode output. As shown, the device consists of a polysilicon disk suspended by a stem at its center, and enclosed by two polysilicon capacitive transducer electrodes spaced 70 nm from the disk perimeter. To operate the device, a dc-bias voltage V_P is applied to the disk structure, and an ac excitation voltage v_i is applied to one of the two electrodes, where the other one is grounded. Note that since there is no dc current flowing with the dc-bias voltage, there is no dc power consumption. This $V_P v_i$ voltage combination can generate an electrostatic force that drives the disk into vibration mode shape where it expands and contracts uniformly around its perimeter [7], as shown in the ANSYS finite element simulation of Fig. 3(a). The disk motion creates dc-biased time-varying electrode-to-resonator capacitors, which then

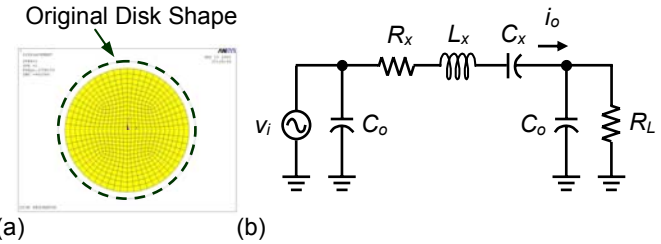

Fig. 3: (a) ANSYS mode-shape simulation and (b) electrical equivalent circuit for a 156- MHz disk resonator.

source output currents i_o that are linear for small motions, but that can contain distortion components when vibration amplitudes are large enough to instigate capacitive transducer nonlinearity. For the measurement setup in Fig. 1(a), this output current can be sensed from the disk structure via a bias-tee. The electrical equivalent model is also shown in Fig. 3(b), where R_x, L_x, and C_x are the motional resistance, inductance, and capacitance, respectively; and C_o is the static electrode-to-disk capacitance.

Fig. 1(b) presents the perspective-view schematic for the same resonator, but this time embedded in the IM_3 signal measurement setup of this work. Unlike the measurement setup of [4], where a power combiner is used to combine two off-resonance electrical interferer tones, these tones are now applied to two separate electrodes. Like the setup of Fig. 1(a), the output current is still sensed from the disk structure via a bias-tee. This measurement setup is superior to that of [4], because it dispenses with the input power combiner, thereby removing its nonlinearities and allowing a much cleaner measurement of device IM_3 components.

To derive the IM_3 force component, a procedure similar to that of [4] can be used. First, the total force generated between the electrode and the disk can be expressed by

$$\begin{aligned} F_{tot} &= \frac{1}{2}(V_P - v_i)^2 \frac{\partial C}{\partial r} = \frac{1}{2}(V_P - v_i)^2 \frac{\partial}{\partial r}\left[C_o \left(1 - \frac{r}{d_o}\right)^{-1} \right] \\ &= \frac{1}{2}(V_P - v_i)^2 \left(\frac{C_o}{d_o}\right) \cdot \left[1 + \frac{2}{d_o} r + \frac{3}{d_o^2} r^2 + \frac{4}{d_o^3} r^3 + \cdots \right] \end{aligned} \qquad (4)$$

where d_o is the static electrode-to-resonator gap spacing. When two electrical interferer tones at ω_1 and ω_2 spaced from the resonant frequency ω_o by $\Delta\omega$ and $2\Delta\omega$, respectively, are applied to the input electrodes, the effective excitation voltage can be expressed as

$$v_i = V_1 \cos\omega_1 t + V_2 \cos\omega_2 t \qquad (5)$$

and the induced mechanical displacements can be written as

$$r = X_1 \cos(\omega_1 t + \phi_1) + X_2 \cos(\omega_2 t + \phi_2) \qquad (6)$$

where approximations to the values of X_1, X_2, ϕ_1, and ϕ_2 can be obtained from the linear voltage-to-displacement transfer function of the resonator

$$\frac{X(j\omega)}{V(j\omega)} = \frac{V_P}{k_{re}} \cdot \left(\frac{\partial C}{\partial r}\right) \cdot \Theta(\omega) \cong \frac{V_P}{k_{re}} \cdot \frac{C_o}{d_o} \cdot \Theta(\omega) \qquad (7)$$

where

$$\Theta(\omega) = \frac{1}{1 - (\omega/\omega_o)^2 + j(\omega/Q\omega_o)} \qquad (8)$$

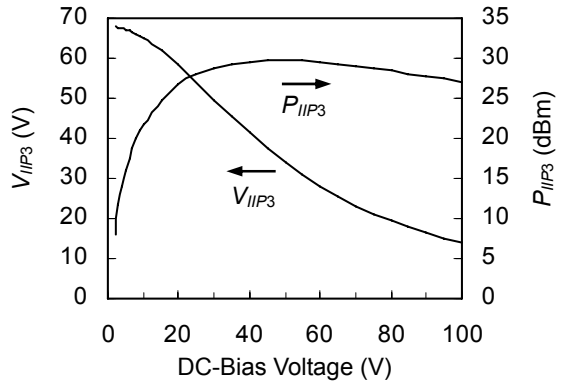

Fig. 4: Simulated V_{IIP3} and P_{IIP3} versus dc-bias V_P applied to a 156-MHz disk resonator with Q = 20,000.

and where k_{re} is the effective stiffness at any location on the disk perimeter.

Applying (5) and (6) to (4) with $V_1 = V_2 = V_i$, then expanding and collecting only IM_3 terms (associated with V_i^3 term) and with frequency ($2\omega_1$-ω_2), the expression for IM_3 force is

$$F_{IM3} = V_i^3 \cdot \left[\begin{array}{l} \frac{1}{2}\frac{\varepsilon_o^2 A_o^2}{d_o^5}\frac{V_P}{k_{re}}\Theta_1 + \frac{1}{4}\frac{\varepsilon_o^2 A_o^2}{d_o^5}\frac{V_P}{k_{re}}\Theta_2^* + \frac{3}{4}\frac{\varepsilon_o^3 A_o^3}{d_o^8}\frac{V_P^3}{k_{re}^2}\Theta_1^2 \\ \frac{3}{2}\frac{\varepsilon_o^3 A_o^3}{d_o^8}\frac{V_P^3}{k_{re}^2}\Theta_1\Theta_2^* + \frac{3}{2}\frac{\varepsilon_o^4 A_o^4}{d_o^{11}}\frac{V_P^5}{k_{re}^3}\Theta_1^2\Theta_2^* \end{array} \right] \quad (9)$$

where ε_o is the permittivity in the gap (in this case, the permittivity of vacuum); $A_o = \pi Rh$ is the electrode-to-resonator overlap area; R and h are disk radius and thickness, respectively; $\Theta_1 = \Theta(\omega_1)$; and $\Theta_2 = \Theta(\omega_2)$.

When (9) is equated with the fundamental force component

$$F_{fund} = V_i \cdot V_P \frac{\partial C}{\partial r} \cong V_i \cdot V_P \frac{\varepsilon_o A_o}{d_o^2} \quad (10)$$

V_i then equals V_{IIP3}, the input voltage magnitude at the IIP_3. Equating (9) and (10) and solving for $V_i = V_{IIP3}$ yields

$$V_{IIP3} = \left[\begin{array}{l} \frac{1}{2}\frac{\varepsilon_o A_o}{d_o^3}\frac{1}{k_{re}}\Theta_1 + \frac{1}{4}\frac{\varepsilon_o A_o}{d_o^3}\frac{1}{k_{re}}\Theta_2^* + \frac{3}{4}\frac{\varepsilon_o^2 A_o^2}{d_o^6}\frac{V_P^2}{k_{re}^2}\Theta_1^2 \\ + \frac{3}{2}\frac{\varepsilon_o^2 A_o^2}{d_o^6}\frac{V_P^2}{k_{re}^2}\Theta_1\Theta_2^* + \frac{3}{2}\frac{\varepsilon_o^3 A_o^3}{d_o^9}\frac{V_P^4}{k_{re}^3}\Theta_1^2\Theta_2^* \end{array} \right]^{-1/2} \quad (11)$$

The expression for power IIP_3 then follows as

$$P_{IIP3} = \frac{V_{IIP3}^2}{2R_T} \quad (12)$$

where R_T represents the total load resistance presented to the measurement instrument. $R_T = R_x$+50Ω in the measurement setup of Fig. 1(b). Of the five terms in (11), the first two derive mainly from nonlinear interactions between applied voltages, whereas the last three are more displacement-dependent, so become more influential as displacements increase.

Fig. 4 plots V_{IIP3} and P_{IIP3} versus dc-bias V_P. Here, V_{IIP3} is seen to decrease monotonically with increasing V_P, as larger displacements generate a larger IM_3 force. In contrast, P_{IIP3} takes on a maximum value at $V_P \sim 50$ V, and then decreases afterwards. The reasons: When V_P is small (e.g., $V_P < 50$ V), V_{IIP3} is dominated by the first two terms in (11), which are not V_P dependant. In this case, the decrease in V_{IIP3} is slower than that of R_x, hence, P_{IIP3} increases with increasing V_P. As V_P becomes large (e.g., $V_P > 50$ V), V_{IIP3} is dominated by the last

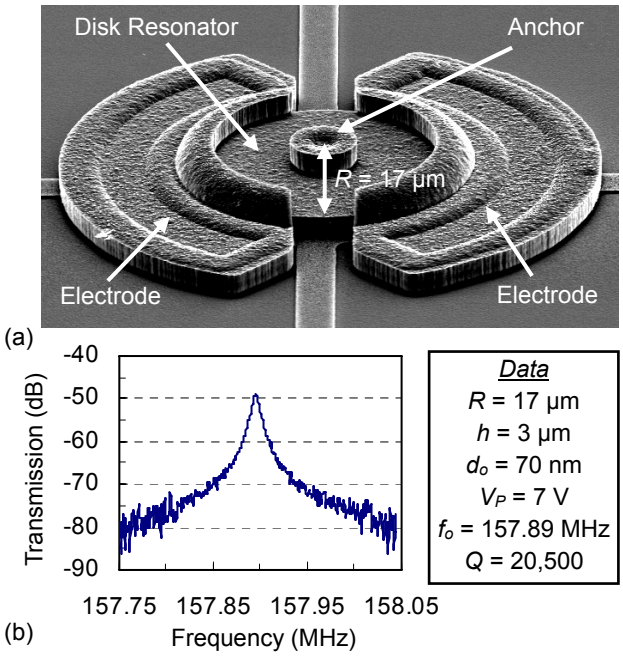

Fig. 5: (a) SEM and (b) measured frequency response (using the setup shown in Fig. 1(a)) for a 156-MHz disk resonator.

three terms in (11), which are strong functions of V_P (since they are displacement-dominated). Thus, for this range of V_P's, V_{IIP3} decreases faster with V_P than R_x, hence, P_{IIP3} decreases with increasing V_P. It should be noted that the dc-bias of 50 V yielding an optimal P_{IIP3} for the present disk resonator is much larger than the 8 V that optimized the 10-MHz beam resonator of [4], mainly due to the larger stiffness of the disk resonator. In practice, system considerations will often limit V_P to less than 10 V, putting disk devices in a regime where P_{IIP3} can be increased by reducing R_x.

IV. Fabrication And Experimental Results

The 60-MHz, 100-MHz, and 156-MHz capacitively transduced contour-mode disk resonators measured in this work were all fabricated via a polysilicon-based, self-aligned, fully-planar wafer-level surface-micromachining process previously used in [7]. The non-intrusive nature of the capacitive transducers used in this work offers the advantage of resonator geometries for which frequency is mainly determined by lateral dimensions; in this case, the disk radius. Thus, unlike most piezoelectric devices, for which lateral dimensions do not directly influence resonance frequency, a single fabrication run with a single structural layer deposition step can yield resonators covering a very diverse frequency range, all specified by CAD layout. Needless to say, this is quite desirable for future multi-band reconfigurable wireless applications [3].

Fig. 5(a) presents the SEM of a fabricated 156-MHz micromechanical contour-mode disk resonator, and Fig. 5(b) presents its measured frequency characteristic (under vacuum) using the setup shown in Fig. 1(a), showing f_o = 157.89 MHz and Q = 20,500.

For IM_3 signal testing, the setup shown in Fig. 1(b) is used with $\Delta\omega = 2\pi\times$(200kHz). In other words, two electrical interferer tones at f_o-200kHz and f_o-400kHz, are applied to two separate input electrodes, where they interact with their own

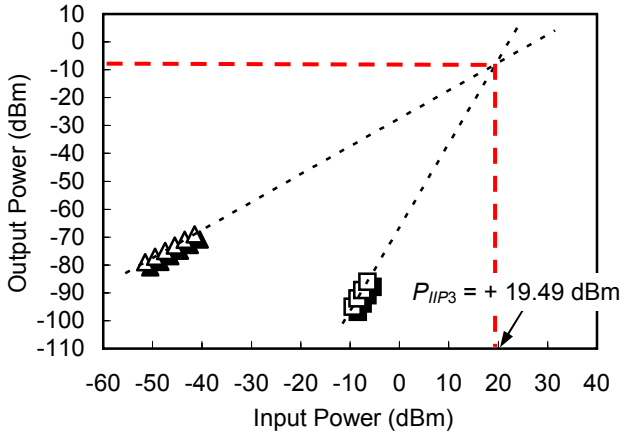

Fig. 6: Measured plots of output power (both fundamental and IM_3) versus input power for a 156-MHz micromechanical disk resonator.

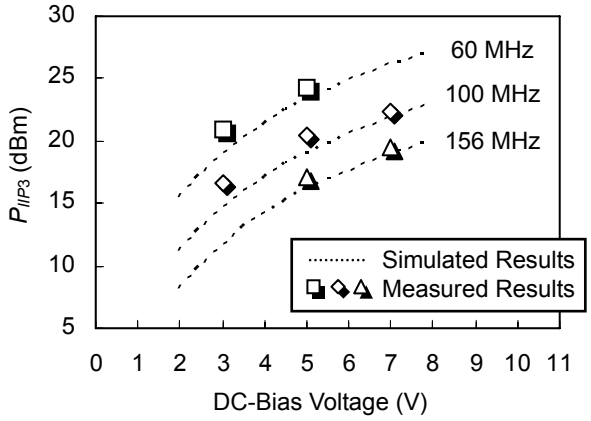

Fig. 7: Measured and simulated values of P_{IIP3} versus dc-bias V_P for 60-MHz, 100-MHz, and 156-MHz contour-mode disk resonators.

induced mechanical displacements to generate third-order intermodulation forces within the resonator passband, that are then detected by a spectrum analyzer at frequencies near f_o. In the actual setup, one of the electrical interferer tones is supplied by a network analyzer, which sweeps over a small frequency span (e.g., 50 kHz around f_o-200kHz), tracing out an IM_3 signal peak in the vicinity of the resonance frequency f_o detected via a spectrum analyzer in MAX HOLD mode [8].

Fig. 6 plots the fundamental and IM_3 output components versus input power for a 156-MHz contour-mode disk resonator biased at 7 V with Q = 20,500. (Note that the input power shown in the horizontal axis of Fig. 6 has already been calibrated from the power supplied by the signal generator to the actual power into the resonator.) From the intersection point in Fig. 6, the P_{IIP3} is seen to be 19.49 dBm, which is quite close to the value of 18.95 dBm predicted by (11).

To further verify the accuracy of the formulation in Section III, Fig. 7 plots measured and simulated values of P_{IIP3} versus V_P for 60-MHz, 100-MHz, and 156-MHz contour-mode disk resonators. As shown, P_{IIP3} increases with increasing resonator dc-bias voltage (as predicted in Fig. 4), where measured P_{IIP3}'s of 16.7 dBm, 20.5 dBm, and 22.4 dBm for a 100-MHz contour-mode disk resonator under dc-biases of 3, 5, and 7 V, respectively; match well with the predicted curve. In addition, Fig. 7 also indicates an increase in P_{IIP3} with increasing resonator size, verified by measured of P_{IIP3}'s of 24.2 dBm, 20.5 dBm, and 17.1 dBm for 60-MHz, 100-MHz, and 156-MHz contour-mode disk resonators with radii of 44 μm, 26 μm, and 17 μm, respectively, at V_P = 5 V. Table 1 summarizes predicted and measured IIP_3 data for the 156-MHz contour-mode disk.

TABLE 1. Contour-Mode Disk Resonator IIP_3 Data

Parameters	156-MHz Disk Resonator	Units
Disk Radius, R	17	μm
Disk Thickness, h	3	μm
Electrode-to-Resonator Gap, d_o	70	nm
DC-Bias Voltage, V_P	7	V
Measured Resonant Frequency, f_o	157.89	MHz
Measured Quality Factor, Q	20,500	—
Predicted Power IIP_3, P_{IIP3}	+ 18.95	dBm
Measured Power IIP_3, P_{IIP3}	+ 19.49	dBm

V. Conclusions

Using an IIP_3 measurement setup that avoids the use of an input power combiner, a 156-MHz contour-mode disk resonator with Q = 20,500 has been demonstrated to have P_{IIP3} = 19.49 dBm, which is substantially better than the -3 dBm previously measured for a 10-MHz clamped-clamped beam resonator, and which now erases skepticism regarding the linearity of micro-scale mechanical resonators. Although the measured IIP_3 is still smaller than that of present-day macroscopic image-reject filters used in cell phone circuits [6], it is still sufficiently large that direct replacement of the latter with a 20 dBm IIP_3 micromechanical version yields a negligible reduction in overall receiver IIP_3 of only 0.11 dB.

Acknowledgment: This work is supported under DARPA Grant No. F30602-01-1-0573.

References:

[1] J. Wang, J. E. Butler, T. Feygelson, and C. T.-C. Nguyen, "1.51-GHz polydiamond micromechanical disk resonator with impedance-mismatched isolating support," *Proceedings*, MEMS'04, Maastricht, The Netherlands, Jan. 2004, pp. 641-644.

[2] S.-S. Li, M. U. Demirci, Y.-W. Lin, Z. Ren, and C. T.-C. Nguyen, "Bridged micromechanical filters," *Proceedings*, IEEE Int. Ultrasonics, Ferroelectrics, and Frequency Control 50th Anniv. Joint Conf., Montreal, Canada, Aug. 2004, pp. 144-150.

[3] C. T.-C. Nguyen, "Vibrating RF MEMS for next generation wireless applications," *Proceedings*, IEEE Custom Integrated Circuits Conf., Orlando, FL, Oct. 2004, pp. 257-264.

[4] R. Navid, J. R. Clark, M. Demirci, and C. T.-C. Nguyen, "Third-order intermodulation distortion capacitively-driven cc-beam micromechanical resonators," *Technical Digest*, MEMS'01, Interlaken, Switzerland, Jan. 2001, pp. 228-231.

[5] A. T. Alastalo and V. Kaajakari, "Intermodulation in capacitively coupled micromechanical filters," *IEEE Electron Device Letters*, vol. 26, no. 5, pp. 289-291, May 2005.

[6] B. Razavi, *RF Microelectronics*, Upper Saddle River, NJ: Prentice Hall, 1998.

[7] J. Wang, Z. Ren, and C. T.-C. Nguyen, "1.156-GHz self-aligned vibrating micromechanical disk resonator," *IEEE Trans. Ultrason., Ferroelect., Freq. Contr.*, vol. 51, no. 12, pp. 1607-1628, Dec. 2004.

[8] A.-C. Wong and C. T.-C. Nguyen, "Micromechanical mixer-filters ("Mixlers")," *Journal of Microelectromechanical Systems*, vol. 13, no. 1, pp. 100-112, Feb. 2004.